Build Simul (2017) 10: 219–227
DOI 10.1007/s12273-016-0319-y

Numerical investigations of the effects of manikin simplifications on the thermal flow field in indoor spaces

Yihuan Yan[1,2], Xiangdong Li[1], Jiyuan Tu[1,2] (✉)

1. School of Aerospace, Mechanical and Manufacturing Engineering, RMIT University, PO Box 71, Bundoora, VIC 3083, Australia
2. School of Architecture, Tsinghua University, PO Box 2021, Beijing 100084, China

Abstract

As one of the most basic parameters, manikin body feature could be an important factor influencing the airflow and temperature fields in indoor environments. This study aims to improve the computational efficiency by optimising and simplifying manikin body features. A 3D scanned computer-simulated person (CSP) with extremely detailed body features was employed, followed by two simplified CSP models with different approaches. One of the simplified models was rebuilt based on the skeleton of the 3D scanned model with very limited body features, while the other model was simplified by removing some of the features from the 3D scanned model. All CSPs were tested under quiescent condition, followed by further comparisons under displacement and mixed ventilations. The outcomes indicated that the geometric difference of manikin body would have significant impact on the airflow patterns near manikin bodies, whilst it has very limited influence on the temperature field. The difference of body features could significantly affect the development of thermal plume, which mainly reflected above the manikin head. Also, change of CSP body features due to simplifications may become more sensitive to the predicted results under mixed ventilation, as a result of fewer interactions between the thermal plume and injected airflow.

Keywords

computer-simulated person (CSP),
CFD,
thermal plume,
indoor air quality

Article History

Received: 14 January 2016
Revised: 25 July 2016
Accepted: 3 August 2016

© Tsinghua University Press and Springer-Verlag Berlin Heidelberg 2016

1 Introduction

Indoor air quality and its potential impacts on the occupational health and safety are of increasing interests in recent years since most people spend over 85 percent of their time indoors (Lai et al. 2000; Salmanzadeh et al. 2012). The occupant bodies are expected to be the key factor affecting the thermal airflow patterns in built indoor spaces. In order to assist the investigations of occupant related thermal airflow characteristics in relation to the air quality, thermal comfort and potential indoor health risks, the inclusion of computer-simulated person (CSP) is essential in computational fluid dynamics (CFD) simulations.

Most of the CSP models employed in the early of 2000s were extremely simple models that only contained the key outlines of human body (Myrakami et al. 2000; Hyun and Kleinstreuer 2001; Hayashi et al. 2002). Extremely simple CSPs were widely employed to simulate multi-occupants indoor environments such as the hospital, classroom and public transports (Poussou et al. 2010; Qian et al. 2008), in order to minimise the computational cost. However, by using these CSPs, simulations could not be able to capture and predict detailed and accurate airflow and temperature characteristics at the interested regions very close to the occupant bodies (e.g. breathing zone). As a temporary solution, the applied CSP models were lately improved with local refinement at corresponding body segments such as the head (Zhu et al. 2005; King Se et al. 2010). These local refined CSPs were mostly used to study the respiratory system related behaviours, which requires detailed facial features of occupants in order to provide detailed airflow information at the nostrils (Li et al. 2016). Although this type of CSPs was beneficial to the local predictions, it was very time consuming to partially refine the CSP models and thereby was not widely applied. In recent years, a new type of CSP model that contains very detailed body features

E-mail: jiyuan.tu@rmit.edu.au

was increasingly used in some up to date researches (Nilsson et al. 2007; Martinho et al. 2012). The 3D scanned CPS provided full body features and very detailed geometry information, but it requires very fine grid to capture the surface features. The computational capacity would be the main barrier for further applications when the number of the 3D scanned CSPs is large and the computational domain is enlarged. In order to conduct simulations with a large number of CSPs, simplifications on the applied CSPs are necessary and a proper approach to simplify CSPs is strongly required.

Therefore, for the purpose of reducing computational cost without significantly scarifying the numerical accuracy, this study aimed to assess the influence of CSP simplifications on the thermal airflow field using two simplified CSP models and to provide recommendations for future applications. The 3D scanned CSP was initially employed to verify the reliability of CFD models. Then, two approaches were used to simplify and optimise the 3D scanned CSP model. The simulation results obtained from these developed CSP models were compared with the original CSP model in terms of airflow field and temperature profiles. The simplified CSP model with better accuracy and good computation efficiency would be recommended for future applications into multi-scale simulations that contains a large number of CSP models.

2 Numerical methods

2.1 Computational domain

The computational domain was based on the experimental setups and measurements with sitting manikin by Licina et al. (2014). The chamber environment was controlled to be quiescent during the experiment. In order to verify the numerical results, case 1 was set accordingly to Liciana et al.'s experiment. The computational domain with dimensions of 4 m-length, 3 m-width and 2.6 m-height was tested to be sufficient to meet quiescent condition, as given in Fig. 1. The front/back and side walls of the computational domain were set as openings with zero pressure to allow airflow in and out freely, while the air temperature inside the domain was the same as the experimental condition (26 °C). The surface area of the manikin model was controlled to be the same as the experimental manikin. The rate of total heat loss from the body was 89 W/m^2 in Licina et al.'s experiment. Since the rate of convective body heat loss governs around 40% of the total heat loss (Myrakami et al. 2000; Sorensen and Voigt 2003), the convective heat flux of 35.6 W/m^2 was applied at the manikin skin while heat transfer by radiation was not included.

In order to further test the influence of the CSPs on the thermal airflow field under ventilated conditions, simulations

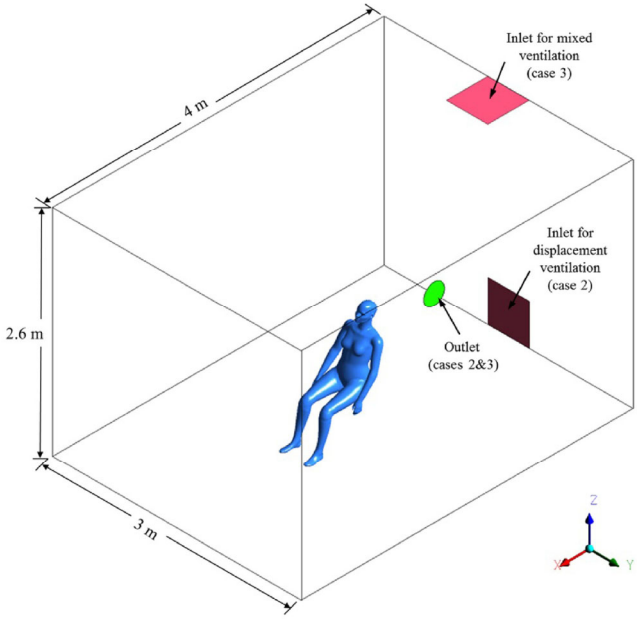

Fig. 1 Computational domain with case 1: quiescent condition; case 2: displacement ventilation; and case 3: mixed ventilation

were also conducted with two different ventilation schemes (i.e. the displacement (case 2) and mixed (case 3) ventilations). As illustrated in Fig. 1, the inlet airflow with velocity of 0.15 m/s was released from a square plane (0.25 m^2) behind the sitting CSP at near floor level and at the ceiling, for the displacement and mixed ventilations, respectively. The outlet was set at the top of the left side wall with zero pressure to allow air come in and out freely. The rest of the walls were set as solid walls rather than openings in cases 2 and 3. All the tested CSPs were placed at the same location with the same sitting posture in all cases.

2.2 Geometry of computational simulated persons (CSPs)

The manikin model from open database (http://www.ie.dtu.dk/manikin) was employed in this study as the original model (OM). This model was a 3D scanned manikin model that has been widely used in other studies (Nilsson et al. 2007; Li et al. 2015), due to its fully scanned and detailed body features. This CSP was modified in order to achieve the same leaning-back posture as the manikin model in Licina et al.'s experiment (Licina et al. 2014). The numerical outcomes from the original model have been validated in our previous study (Li et al. 2015) through comparing with the experimental measurements by Licina et al. (2014). Therefore, the simulation results from the OM were used as a reference to test other developed CSPs. The mesh decimating approach was initially utilised in our previous study to simplify the CSP model. Although the results proved the significance of body simplification on the thermal airflow predictions, the outcomes were limited

to the mesh decimating approach only and cannot be used to assess those widely used simplification approaches in the literature. Therefore, in order to further investigate the effect of CSP simplification on the thermal airflow field in the indoor spaces, another two simplification approaches that have been widely reported in the literature (Myrakami et al. 2000; Poussou et al. 2010) were employed in this study to simplify the manikin models.

The first method (Ruzic and Bikic 2014) was to completely rebuild the manikin model by following the same skeleton as the 3D scanned model (RM), as provided in Fig. 2. The core skeleton structure from the 3D scanned model was extracted and applied as the reference to create the new model. The RM contains more regular surface curves and simpler body features, whilst very detailed body features were eliminated.

The second simplification approach was to maintain the overall body features of the 3D scanned model, but removing some insignificant features that have very limited impacts on the simulation results. It can be seen from Fig. 2, the ears, eyes and mouth from the original 3D scanned model were eliminated from the simplified and smoothed model (SM). Also, redundant features such as the abnormal segment on the fingertips were further removed by smoothing the manikin surface to reduce unnecessary grids.

2.3 Numerical producers

The commercial CFD software CFX 14.5 (Ansys) was employed to fulfill the simulations. The RNG k–ε turbulence model was applied in this study due to its high reputation on predicting three-dimensional airflow field in indoor environments (Chen 1995; Chen et al. 2006). The discretisation for advection terms was based on the high order advection scheme to achieve better robustness and accuracy, while the SIMPLEC algorithm was applied to solve the pressure–velocity coupling. The scalable wall function was employed to resolve the boundary layer at near-wall regions. The computational domain and manikin surfaces were discretised using unstructured tetrahedral grids in the commercial software ICEM 14.5 (Ansys). Each CSP was computed under various combinations of grid sizes (e.g. OM with maximum surface elements of 5 mm and OM Coarse with maximum surface elements of 10 mm) to test and check the sensitivity of the grid size. The grid independence tests for all CSPs were conducted by checking the mesh quality in ICEM (Ansys) and the grid convergence index (GCI) (Roache 1994; Eça and Hoekstra 2014). The overall mesh quality and GCI was controlled to be similar at the OM, RM and SM cases and the $y+$ values for all CSPs were controlled to be below 3. The tested grid number and size at bulk region were set to be uniform when testing different manikin models. Detailed grid information such as the number of grid for each studied case was in Table 1. The convergence with the residual less than 1×10^{-6} of the continuity equation was achieved within 1500 iterations.

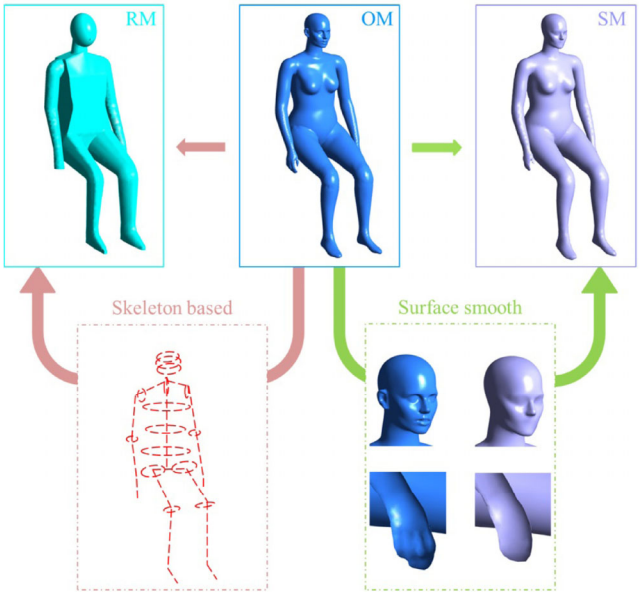

Fig. 2 The schematic views of the rebuilt manikin (RM) model (on the left), 3D scanned original manikin (OM) model (in the middle) and the simplified and smoothed manikin (SM) model (on the right).

Table 1 Grid information of different CSPs

No. of grid	OM	OM Coarse	RM	RM Coarse	SM	SM Coarse
Head	52204	13210	6970	3669	12440	6424
Neck	3169	912	459	238	812	602
Upper body	14832	3776	2184	2968	3603	1879
Arms & hands	10297	2503	1349	1539	2470	1247
Legs & feet	21606	5296	2454	1161	5343	3879
Total no. of grid at manikin surface	1.0×10^5	2.6×10^4	1.3×10^4	9.6×10^3	2.5×10^4	1.4×10^4
Total no. of grid of the whole domain	2.95×10^6	2.65×10^6	2.51×10^6	2.45×10^6	2.63×10^6	2.54×10^6

3 Results and discussion

3.1 Quiescent condition (case 1)

The numerical results regarding the global and local airflow field of the OM case was firstly presented and compared to the experimental measurements to validate the computational reliability. Globally, the overall velocity contour in front of the sitting manikin model obtained from the simulation was compared with the measurement by Licina et al. (2014) in Fig. 3(a). Also, the comparison of velocity contour in

conjunction with the velocity vector at the breathing zone of manikins was provided in Fig. 3(b). As can be seen in Fig. 3(a), the predicted velocity contour using OM in front of the sitting manikin body yielded very similar ascending airflow pattern to the experimental measurement. The results were slightly different in the regions far away from the manikin body. The experimental results seemed to be less consistent in some bulk regions, probably due to the fact that the PIV images were not taken simultaneously during the experiment. For the airflow field in manikin breathing zone, the experimental measurements indicated very strong effect of buoyancy driven thermal plume generated by body heat that carries the air in the vicinity of manikin body traveling upward. This characteristic of airflow was also accurately predicted by the simulation, as shown in Fig. 3(b). Overall, the CFD approach (OM) predicted very similar results of the airflow field to the experimental measurements and the reliability of simulation was thereby validated. Further validations can be found in the published study using the same 3D scanned model and similar numerical setups (Li et al. 2015).

For the purpose of quantitative comparison, velocity profiles from various lines were extracted from each of the case and compared. As illustrated in Fig. 4 (*X*-*Z* plane view), three lines (L1, L2 and L3) were selected from the floor to the ceiling with same incline angle as the sitting manikin body. From the top view (*X*-*Y* plane) in Fig. 4, line 4 (L4) was selected to be half meter above the manikin head to capture the local of peak velocity, as well as the axially velocity distribution. The horizontal velocity profile just in front of the manikin nose was extract by line 5 (L5). Three additional cases (OM Coarse, RM Coarse and SM Coarse) were

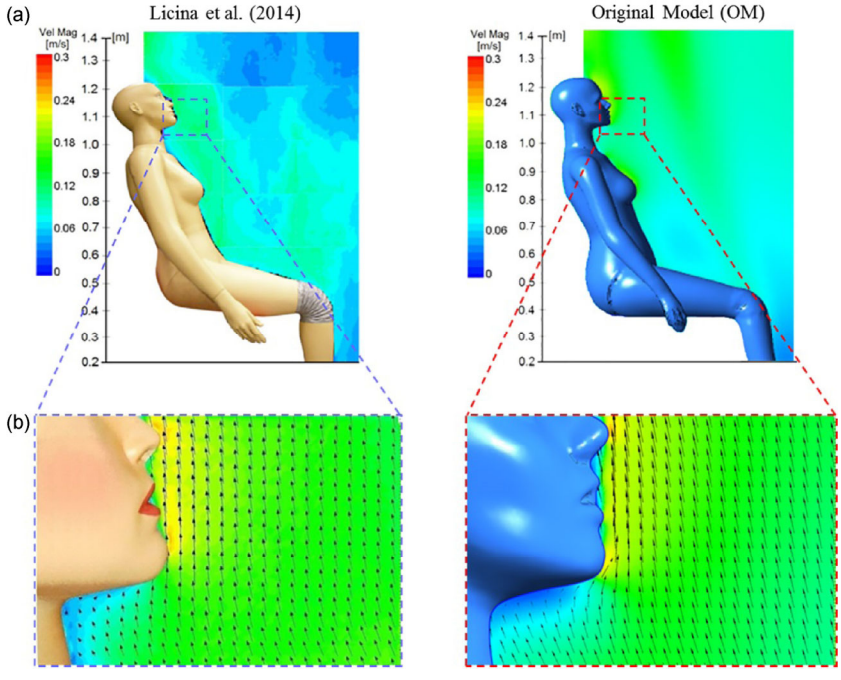

Fig. 3 Comparison of (a) the overall velocity contour in front of the sitting manikin; (b) the velocity contour and velocity vector at breathing zone between the experimental (left) and the simulation (right) results

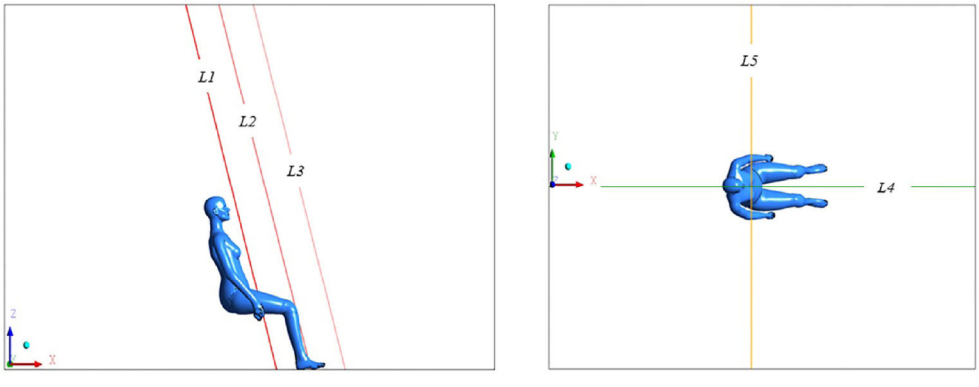

Fig. 4 Positions of selected lines with side view (*X*-*Z* plane) and top view (*X*-*Y* plane)

computed when comparing the velocity distributions along various locations. Each of these cases was computed with slightly coarsened finish. With the coarse model, much lower number of grids was required to compute the manikin surface, as listed Table 1. The mesh qualities for all the coarse models were still controlled to be uniform. The purpose of adding coarsened CSPs is to test the influence of CSP simplifications on the mesh sensitivity.

The results along L1 given in Fig. 5 shows that from the ground level to the height of sitting manikin (0–1.2 m), the velocity profiles were very close among these six cases. At the region above the manikin head (above 1.2 m), the SM case was able to predict similar velocity profiles as the OM case, whereas the RM model predicted significantly different velocity distributions. The peak velocities at L1 predicted by the OM and SM models were 1.84 m/s and 1.78 m/s at height of 2.1 m, respectively. The difference of peak velocity between these two models was under 3%. On the other hand, the maximum velocity in RM model occurred at lower position (1.7 m) with magnitude of 0.14 m/s, which was dramatically different to the other models. L2 was showing a similar trend of velocity distribution as L1, while the difference between RM and the other cases was less significant. In the bulk region (L3), the velocity profiles were almost the same among various cases, although the velocities were still different at the ceiling level. Thus, the effect of manikin body regarding the airflow field would be significant in the vicinity of manikin body, but less obvious at bulk regions below manikin height. In terms of the bulk region above the manikin head, Fig. 5 (L4) shows that the velocity difference occurred from about 1.5 m to 2.25 m, along *X*-axis, which is almost the region where the thermal plume effect is maximised. At the rest plots away from the thermal plume region, velocity distributions were predicted to be similar. Thus, the change of manikin body features would significantly affect the airflow field at the region above the manikin body where the thermal plume effect is strong. For the horizontal velocity distribution in front of the manikin nose (L5 in Fig. 5), the predicted velocity profiles by different cases only vary in the vicinity of the manikin head with a diameter of 0.5 m. Since the thermal plume affected airflow was travelling mainly upward, the velocity difference along L5 could be mainly caused by the geometric difference of each model, which is insignificant from the observation of the plots.

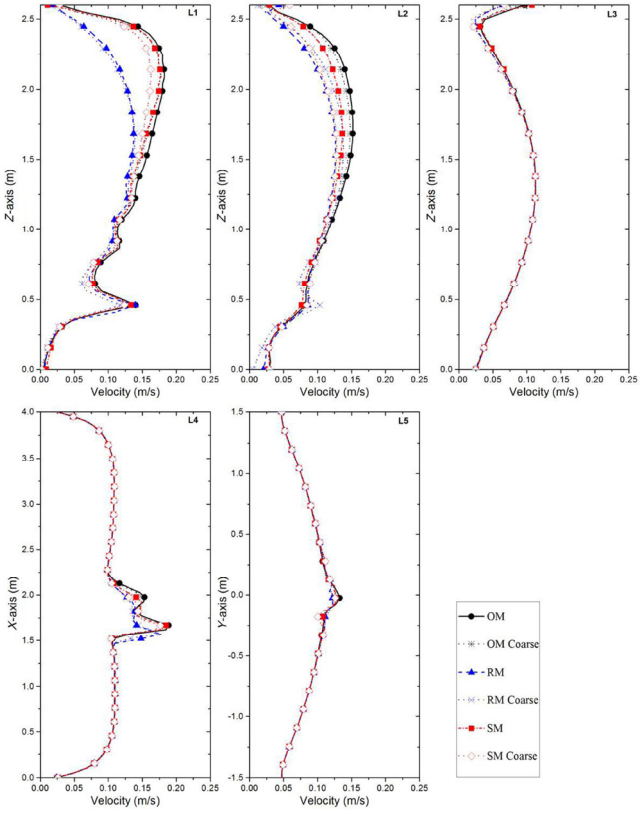

Fig. 5 Velocity profiles along selected lines

When comparing each case with its coarsened model, it can be seen from Fig. 5 (L1 and L2) that the velocity predictions were very stable between the RM and RM Coarse cases, although the RM model did not agree well with other models. This indicated that the skeleton based simplifications had less impact on the mesh sensitivity. On the contrary, for the SM model which obtained closer results to the OM case, the numerical outcomes would be very sensitive to the simplification level and mesh quality.

Also, the temperature contours of three studied cases were compared in Fig. 6. All cases predicted very obvious thermal plume above the manikin heads, while less obvious thermal plume development can be noticed above the manikin knees. However, the developing pattern of thermal plume from the RM case was slightly different to the other two cases. The backward development of thermal plume predicted by the RM case was more significant. This could be caused by the change of surface features and projection curves of the RM case. The secondary thermal plume generated by the heat of lower manikin body travelled upward with similar pattern as the major one in same case but less intense.

3.2 Displacement and mixed ventilations (Cases 2 and 3)

The influence and significance of the CSP simplification on the airflow field may vary when the ventilation schemes changes. The simplified CSPs (RM and SM) were further compared to the original model under the displacement and mixed ventilations that are the most commonly used ventilation schemes in indoor spaces such as office, classroom and etc. Since the aforementioned results indicated that the

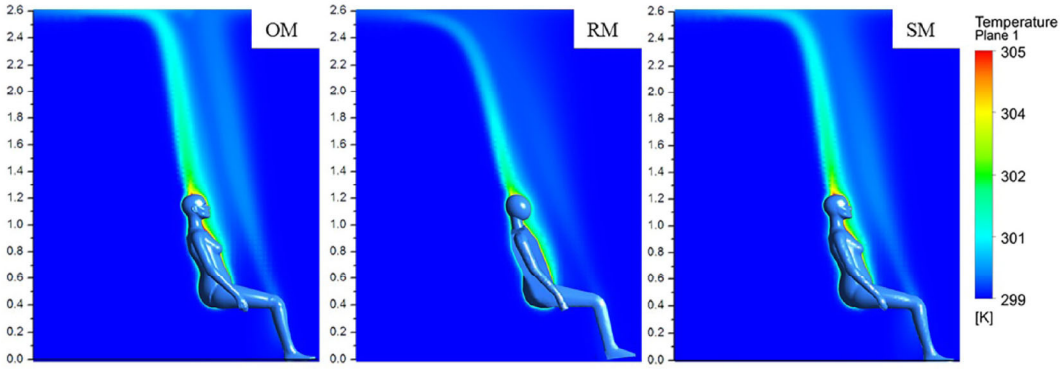

Fig. 6 Temperature contour for studied cases

CSP simplification had higher impact on the airflow field than the temperature profiles, focused were drawn mainly on the velocity field after the HVAC system was considered.

The velocity vectors representing the overall airflow patterns predicted by all the CSP cases under different ventilations were compared at the mid-plane (*X*-*Z* plane), as shown in Fig. 7. Under the displacement ventilation system, the inlet airflow travelled horizontally across the near-floor region until it reached the thermally affected region in the vicinity of the sitting CSP. By interacting with buoyancy driven thermal plume, injected airflow at relatively higher level was interrupted and changed its direction from horizontal to nearly vertical. Obvious ascending pattern of the airflow can be observed in front of and above the CSP body. The air exchange rate is relatively higher at the occupant's breathing zone under displacement ventilation thanks to the interactions between the injected airflow and the thermal plume, although this may potentially brought near-floor level contaminants into the breathing zone as well. On the other hand, when the ventilation was switched to the mixed scheme, the airflow field completely changed. Since the inlet velocity was not significantly high, after reaching the floor, the injected airflow quickly dispersed and stayed at the near-floor level, which suppressed its interactions with the thermal plume generated by the heated CSP. As a result, the airflow was divided into two main streams by the injected

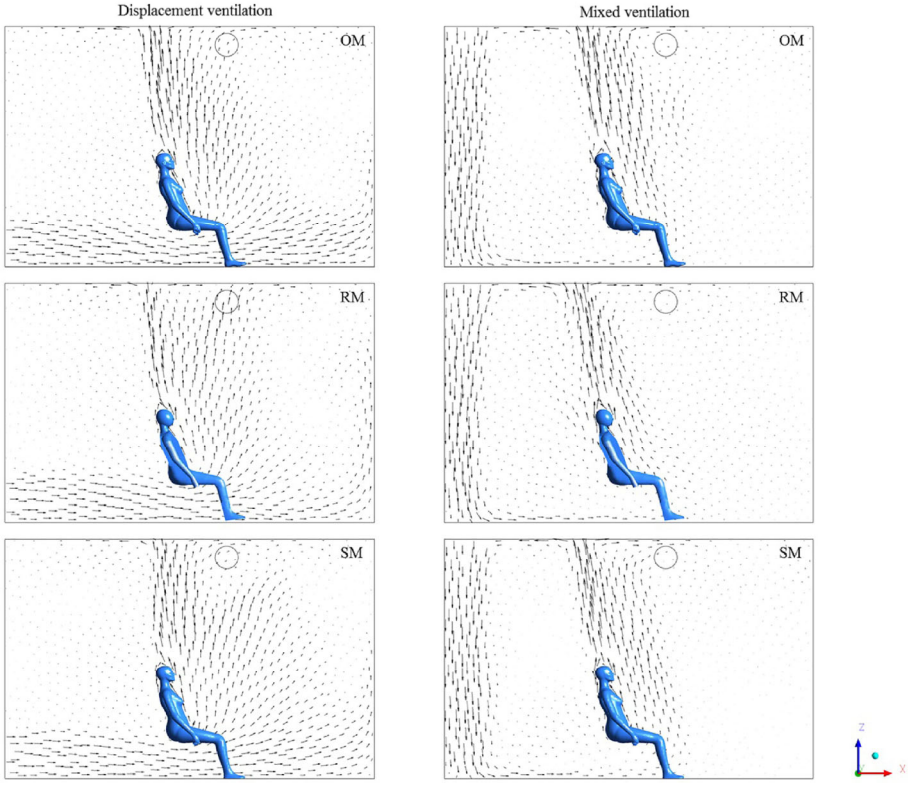

Fig. 7 Velocity vectors predicted by different CSPs under the displacement (left) and mixed (right) ventilations

airflow and thermal plume, respectively, which was not ideal for even air distribution and exchange.

By comparing the predicted airflow field using various CSPs, the impact of the body simplifications on the airflow field can be clearly visualised under both ventilation schemes, as demonstrated in Fig. 7. With the displacement ventilation, it seemed that the change of body features had less impact on the over airflow pattern than that with mixed ventilation. This is probably because that the airflow velocity around the sitting CSP was relatively high and thereby the effect of the thermal plume became less significant. In terms of the mixed ventilation, the predicted velocity around the CSP by the SM case agreed better to the OM than that of the RM case. Both OM and SM cases obtained relatively wider thermally affected region around the CSPs than the rebuilt model.

The quantitative velocity profiles at the same selected lines as aforementioned (Fig. 4) were compared among all the CSPs under studied ventilations. Under displacement ventilation, it can be noticed from Fig. 8 that the plotted velocity profiles by the SM case were very close to the original model, despite some minor differences at L2. The skeleton based rebuilt CSP case, on the other hand, failed to predict similar local velocity distributions to the OM case particularly at L2 and L3, although it agreed well with the original model on the global velocity distributions. It seemed that the impact of body simplification was quite significant at L2, which was placed 25 cm in front of the CSP upper torso, while it also had considerable influence on the other two lines (L1 and L3) inside the thermally affect regions. After changing the ventilation to mixed scheme, the deviations of velocity profiles (Fig. 9) at L2 from both SM and RM cases were enlarged, although the velocity patterns were remained similar among all studied CSPs. Despite that, under mixed ventilation scheme, the RM case also failed to capture the similar velocity profiles along the longitudinal direction (L4), in which the deviation still occurred at the thermally affected region very close to the CSP body. Therefore, according to the comparison, it can be concluded that the SM model was more promising to predict similar airflow profiles globally and locally to the original model than the rebuilt model, while the influence of CSP simplifications was more obvious under the mixed ventilation scheme.

In terms of the temperature distribution, it can be noticed from Figs. 10 and 11 that the main deviations caused by CSP simplifications occurred at Lines 1 and 2 under both ventilation schemes, whereas the temperature profiles were not significantly affected by different CSPs along the longitudinal direction (Line 4) and the horizontal direction (Line 5). The surface-smoothed CSP (SM) managed to

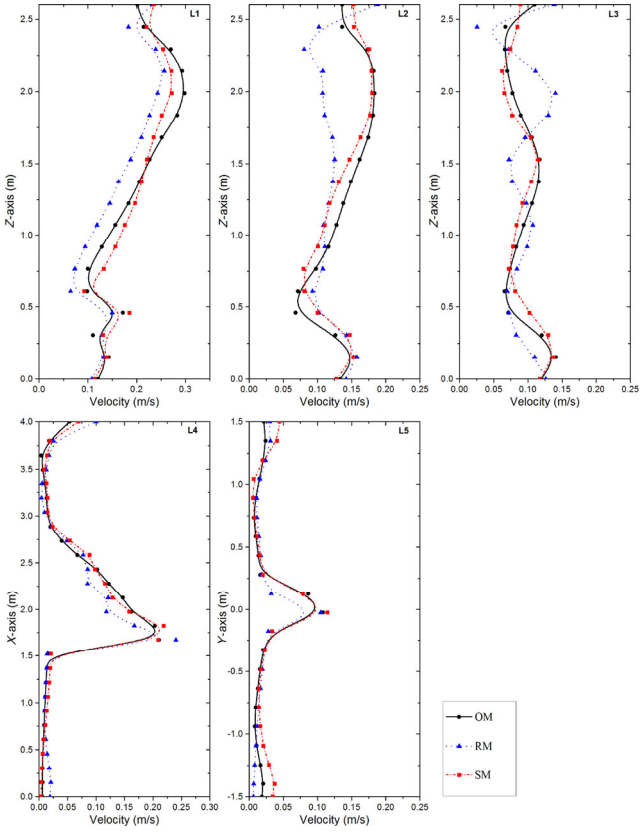

Fig. 8 Velocity profiles at selected lines under displacement ventilation

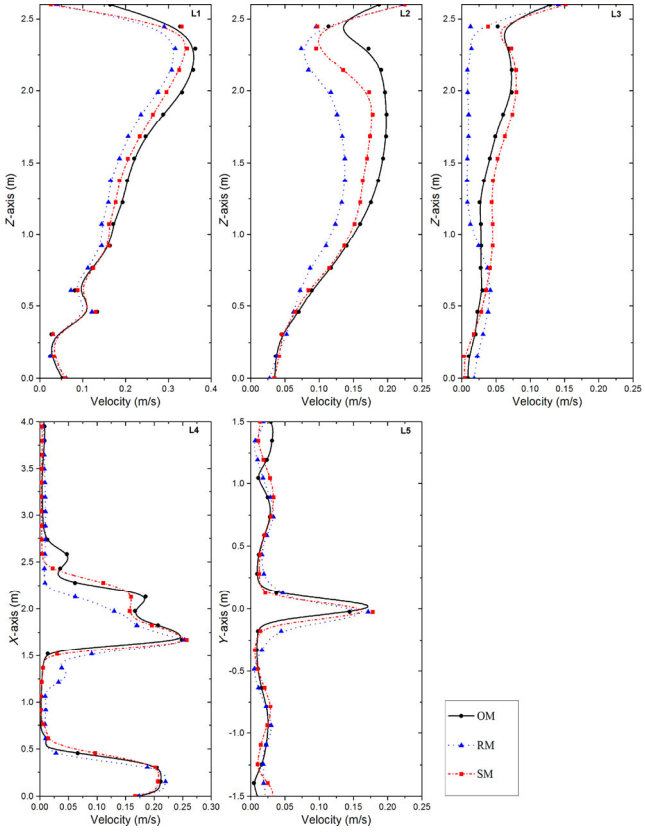

Fig. 9 Velocity profiles at selected lines under mixed ventilation

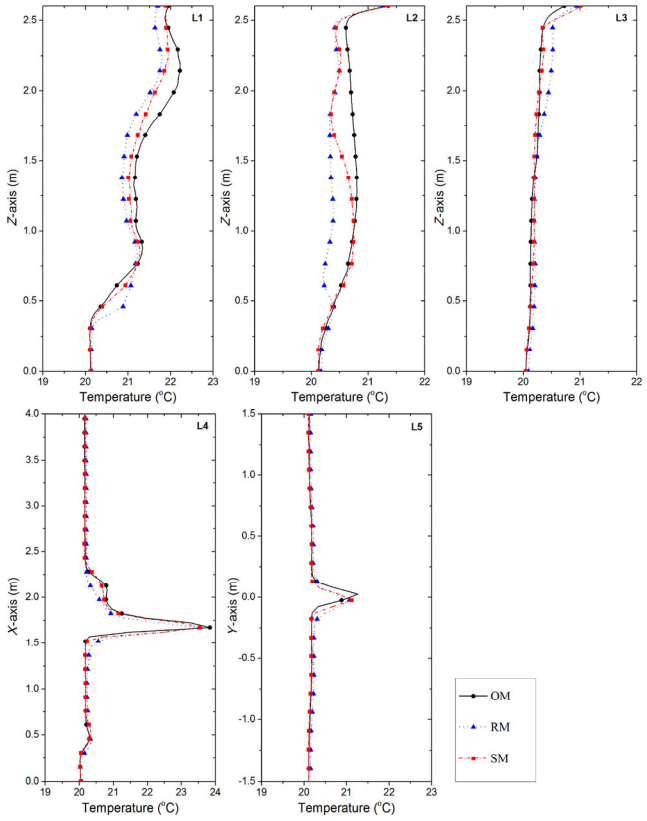

Fig. 10 Temperature profiles at selected lines under displacement ventilation

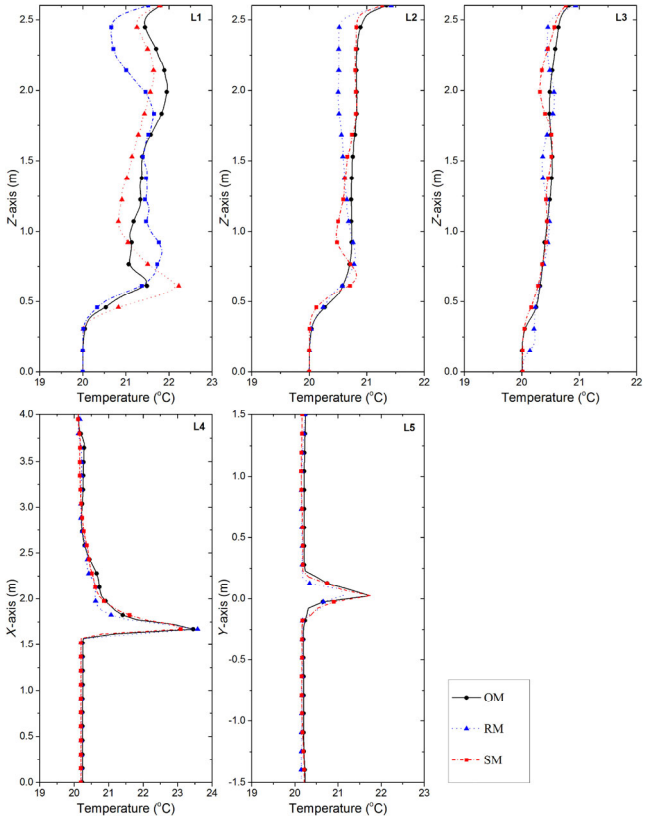

Fig. 11 Temperature profiles at selected lines under mixed ventilation

obtained very close temperature distributions to the original models at all selected lines, although the temperature magnitudes were slightly different (with error less than 3%) at Lines 1 and 2. Under mixed ventilation scheme, the rebuilt model (RM) did not predict very similar temperature distribution to the OM in the vicinity to the CSP (Line 1), which could be caused by the body feature differences at local body segments. Generally, the effects of the CSP simplifications on the temperature fields were less significant than that under the airflow fields.

4 Conclusions

The effect of CSP diversity by simplifications on predicting the thermal airflow fields was studied under quiescent condition, displacement and mixed ventilations. Based on the outcomes, the conclusions rising from this study are as follows.

The geometry of CSP has more significant effect on the local airflow field around the manikin body than that on the temperature distributions. The significance of manikin model variety will be enlarged on top of the manikin head due to the effect of buoyancy driven thermal plume by body heat, while the locations of the maximum velocity were very sensitive to the applied CSPs.

The SM model is more capable of obtaining reliable and accurate predictions to the original model with reduced computational cost. Thus, the SM model is recommended to replace the original model when studies require very detailed body features. However, the grid independence of this simplification approach is quite sensitive. The skeleton based model (RM), however, was not as good as the SM on predicting the local airflow field, but it required much less computation resource and had better numerical stability. It is preferred for simulations with high amount of CSPs.

The geometrical diversity of CSP caused by simplifications had higher impact on the thermal airflow field under the mixed ventilation than that with displacement ventilation based on the studied cases. This outcome may vary if the vent sizes and positions are changed or the inlet air velocity is different. Since the focus of this study is on the CSP simplification approaches, further test of HVAC systems in conjunction with CSPs will be conducted in the future studies.

Acknowledgements

The financial supports provided by the National Basic Research Program (973) of China (No. 2012CB720100) and

the National Natural Science Foundation of China (No. 21277080) are gratefully acknowledged.

References

Chen F, Yu SCM, Lai ACK (2006). Modeling particle distribution and deposition in indoor environments with a new drift–flux model. *Atmospheric Environment*, 40: 357–367.

Chen, Q (1995). Comparison of different k–ε models for indoor air flow computations. *Numerical Heat Transfer*, *Part B*: *Fundamentals*, 28: 353–369.

Eça L, Hoekstra M (2014). A procedure for the estimation of the numerical uncertainty of CFD calculations based on grid refinement studies. *Journal of Computational Physics*, 262: 104–130.

Hayashi T, Ishizu Y, Kato S, Murakami S (2002). CFD analysis on characteristics of contaminated indoor air ventilation and its application in the evaluation of the effects of contaminant inhalation by a human occupant. *Building and Environment*, 37: 219–230.

Hyun S, Kleinstreuer C (2001). Numerical simulation of mixed convection heat and mass transfer in a human inhalation test chamber. *International Journal of Heat and Mass Transfer*, 44: 2247–2260.

King Se CM, Inthavong K, Tu J (2010). Inhalability of micron particles through the nose and mouth. *Inhalation Toxicology*, 22: 287–300.

Lai ACK, Thatcher TL, Nazaroff WW (2000). Inhalation transfer factors for air pollution health risk assessment. *Journal of the Air & Waste Management Association*, 50: 1688–1699.

Li X, Yan Y, Tu J (2015). The simplification of computer simulated persons (CSPs) in CFD models of occupied indoor spaces. *Building and Environment*, 93: 155–164.

Li X, Inthavong K, Tu J (2016). Numerical investigation of micron particle inhalation by standing thermal manikins in horizontal airflows. *Indoor and Built Environment*, 25: 357–370.

Licina D, Pantelic J, Melikov A, Sekhar C, Tham KW (2014). Experimental investigation of the human convective boundary layer in a quiescent indoor environment. *Building and Environment*, 75: 79–91.

Martinho N, Lopes A, Gameiro Da Silva M (2012). Evaluation of errors on the CFD computation of air flow and heat transfer around the human body. *Building and Environment*, 58: 58–69.

Myrakami S, Kato S, Zeng J (2000). Combined simulation of airflow, radiation and moisture transport for heat release from a human body. *Building and Environment*, 35: 489–500.

Nilsson H, Brohus H, Nielsen P (2007). Benchmark Test for a Computer Simulated Person-Manikin heat loss for thermal comfort evaluation: Version of February 2007. Aalborg University Denmark & Gavle University Sweden.

Poussou SB, Mazumdar S, Plesniak MW, Sojka PE, Chen Q (2010). Flow and contaminant transport in an airliner cabin induced by a moving body: Model experiments and CFD predictions. *Atmospheric Environment*, 44: 2830–2839.

Qian H, Li Y, Nielsen PV, Hyldgaard CE (2008). Dispersion of exhalation pollutants in a two-bed hospital ward with a downward ventilation system. *Building and Environment*, 43: 344–354.

Roache RJ (1994). Perspective a method for uniform reporting of grid refinement studies. *Journal of Fluids Engineering*, 116: 405–413.

Ruzic DA, Bikic SM (2014). An approch to the modelling of a virtual thermal manikin. *Thermal Science*, 18: 1413–1423.

Salmanzadeh M, Zahedi G, Ahmadi G, Marr DR, Glauser M (2012). Computational modeling of effects of thermal plume adjacent to the body on the indoor airflow and particle transport. *Journal of Aerosol Science*, 53: 29–39.

Sorensen DN, Voigt LK (2003). Modelling flow and heat transfer around a seated human body by computational fluid dynamics. *Building and Environment*, 38: 753–762.

Zhu S, Kato S, Murakami S, Hayashi T (2005). Study on inhalation region by means of CFD analysis and experiment. *Building and Environment*, 40: 1329–1336.